ROUGH DRAFT

Sandia Laboratories

SAND79-1918C

Melt/Concrete Interactions: The Sandia Experimental Program, Model Development, and Code Comparison Test*

D. A. Powers and J. F. Muir
Sandia Laboratories
Albuquerque, NM

Presented at the Seventh Water Reactor Safety Research Information Meeting, November 5-9, 1979, Gaithersburg, Maryland.

*This work was supported by the United States Nuclear Regulatory Commission.

In the unlikely event of a class-nine accident at a nuclear power reactor, it is possible that molten fuel and steel from the reactor core will penetrate the reactor pressure vessel and cascade into the reactor cavity. The intense interaction that would develop between the high temperature core materials and the cavity concrete raises a number of safety questions. The nature of melt/concrete interactions during core meltdown accidents must be understood if a realistic evaluation of the risks associated with the use of nuclear power is to be made.

High temperature melt/concrete interactions have been studied both experimentally and analytically at Sandia under sponsorship of Reactor Safety Research of the U. S. Nuclear Regulatory Commission. The purpose of these studies has been to develop an understanding of these interactions suitable for risk assessment. In this paper, results of the experimental program are summarized and a computer model of melt/concrete interactions is described. A melt/concrete interaction test that will allow this and other models of the interaction to be compared is also described.

The code comparison exercise, using this Sandia test and a similar test at the Kernforschungszentrum Karlsruhe, was suggested during discussions among core-melt researchers from laboratories in both the United States and the Federal Republic of Germany at the December 1978 Fuel Meltdown Program Review and and NRC/FRG Information Exchange Meeting. Its objective is to provide a basis for evaluating the various codes with respect to how well they model the important interaction phenomena and predict critical events.

I. Experimental Program

The experimental program has been directed toward qualitatively identifying important physical and chemical processes that occur during high temperature melt/concrete interactions and quantitatively evaluating those phenomena particularly important for reactor safety considerations. The experimental program has been characterized by the use of prototypic melts and concretes at realistic conditions in large-scale tests. Melts of mild steel, stainless steel, and Corium A+R (54w/o UO_2; 16w/o ZrO_2; 30w/o stainless steel), varying in size from 2 to 220 kg and at temperatures of 1400-3000°C, have been used. In some cases Mo, SrO, SnO_2, Cs_2UO_4, La_2O_3 and, CeO_2 have been added to the melts to simulate fission products. A basaltic and two limestone concretes, representative of concretes in existing or planned nuclear reactors, have been studied in the program. The chemical compositions of these concretes are listed in Table I.

The initial goal of the experimental program was the qualitative identification of phenomena occurring during melt/concrete interactions. These qualitative observations from the experimental program are listed in Table II as a series of comparisons with assumptions made in The Reactor Safety Study (WASH-1400).

Once the qualitative identifications were made, the particularly pertinent phenomena were quantitatively studied. Sustaining melts of up to 220 kg stainless steel by inductive

heating while in contact with concrete, and observing the behavior of thermitically generated melts interacting with concrete by x-ray image intensification, were particularly fruitful avenues for making these quantitative studies. The numerical data generated in the experimental program is listed in Table III and discussed more fully below.

A. Concrete Erosion Rate

A core melt would consist of a metallic phase and an oxidic phase. The metallic phase was found in the experimental program to be far more aggressive toward concrete than the oxidic phase by virtue of its higher thermal conductivity. The rate of erosion of concrete is approximately a linear function of the rate of heat transfer to the concrete as shown in Figure 1. Consequently, the rate of concrete erosion by a melt is a function of the difference between the melt temperature and the onset of melting in the concrete. The variation in erosion rate with this temperature difference is shown in Figure 2. Note that erosion of low melting concretes, such as basalt, can take place even after the core melt has solidified.

Erosion does not occur uniformly about the perimeter of a melt. Gases liberated from the concrete and passing up along the walls of a concrete cavity tend to provide a thermal shield between the walls and the melt. The ratio of horizontal to downward erosion decreases with increasing gas generation rates. This effect can be clearly seen in the comparison of the post-test cavity shapes for the limestone

concrete (high gas generation rate) and basalt concrete (low gas generation rate) crucibles shown in Figure 3. Fully dehydrated and at least partially decarboxylated concretes erode approximately uniformly in the horizontal and downward directions.

B. Gas Generation

Gases are produced during melt/concrete interactions by the thermal decomposition of hydrates and carbonates in the concrete. The decomposition reactions occur in three temperature regimes:

1) loss of "free" water, 30-250°C
2) loss of chemically bound water, 380-550°C
3) loss of carbon dioxide, 680-1000°C

Above 1000°C other constituents of concrete, including Na_2O and SiO, are vaporized.

The rate of gas generation during melt/concrete interaction is not directly related to the rate of concrete erosion. Rather, it is dependent on the rate and extent of heat conduction into the concrete. The kinetics of gas-generating concrete decomposition reactions may be related to temperature and the rate of temperature change by kinetic expressions of the form:

$$\frac{d\alpha}{dt} = k \exp(-E/RT)(1-\alpha)^n$$

where E, k, and n are parameters, α is the extent of reaction, R is the gas constant, t is time, and T is the absolute

temperature. Parametric values found for the decomposition reactions in various concretes are listed in Table IV. The rate expressions have been incorporated in a detailed model of concrete by Knight and Beck.

Aside from influencing the direction of melt attack on the concrete as described above, the gases released from the concrete exert a dominant influence on the melt/concrete interaction. They keep the melt well-stirred, especially the metallic phase, so that the melt is essentially isothermal. The gases also levitate and swell the melt. The extent of this swelling of the melt is a function of the gas generation rate, the melt depth, and the gas hold-up within the melt. Observed melt depths for a shallow pool are plotted versus superficial gas velocity in Figure 4. Swelling of the pool increases almost linerarly with superficial gas velocity until a critical plateau is reached. Further increases in gas generation rate do not influence the observed pool depth.

As the gases liberated from the concrete - primarily CO_2 and H_2O - percolate up through the melt they are chemically reduced by the metallic phase of the melt to hydrogen and carbon monoxide. The resulting oxidation of the metallic species represents a major mechanism for depleting the core melt of its aggressive metallic phase.

The extent of chemical reduction of the concrete gases is controlled by the iron-iron (II) oxide equilibrium. The oxygen fugacities of gases extracted at various temperatures

from above a melt interacting with concrete are plotted along with the iron-iron (II) oxide phase boundary in Figure 5. The gas composition evolves with temperature along this phase boundary. One consequence of this pathway of gas evolution is that the gas becomes rich in methane rather than hydrogen as it cools, as shown in Figure 6.

C Aerosol Generation

Aerosol generation is intense during melt/concrete interactions. The aerosol concentration observed during the course of a transient Corium A+B/concrete interaction is shown in Figure 7. Concentrations in excess of 100 g/m^3 were observed early in the test. Even after about 40 seconds, when the melt had very nearly solidified, aerosol concentrations were about 20 g/m^3. During large-scale steel melt/concrete interactions tests average aerosol concentrations were about 10 g/m^3.

The aerosols have mean aerodynamic particle sizes of 1-2 μm as shown in the distribution plot in Figure 8.

Chemical compositions of aerosols from several tests are listed in Table V. Much of the aerosol comes from non-melt sources - i.e., the concrete. When volatile fission products are present - such as Cs, MoO_3, Sn, and Cd - they make up a significant fraction of the aerosol. Fission products expected to be refractory and present in the metal phase are apparently sparged and oxidized by the gases passing through the melt.

The aerosol concentration observed in the tests is a function of the gas generation rate as shown in Figure 9. Concentration increases approximately linearly with the superficial velocity of gas produced by the melt/concrete interaction. The finite aerosol concentration at zero superficial gas velocity may be attributed to thermal vaporization of species from the melt. This and other aspects of aerosol generation will be discussed more fully in another paper at this conference.

D. Code Comparison Test

The experimental techniques developed in this program will be used to provide test data for comparing computer models of melt/concrete interactions. Code comparison tests will be performed by both Sandia and the Kernforschungszentrum Karlsruhe in West Germany. The test procedure for the Sandia test is shown schematically in Figure 10. About 200 kg of 1700°C stainless steel was deposited into a limestone concrete crucible (concrete III in Table I). The melt was sustained by inductive heating with coils embedded in the concrete.

Data collected in the Sandia test for code comparison purposes were:

1) rate of concrete erosion
2) extent of concrete erosion
3) rate of metal oxidation during the interaction
4) rate of melt solidification
5) concrete temperatures.

Additional data produced during the test that will allow evaluations of future improvements in the computer models include:

1) aerosol composition
2) aerosol generation rate
3) gas composition
4) gas generation rate
5) upward heat flux due to radiation and convection
6) moisture migration within the concrete
7) mechanical response of the concrete
8) melt temperatures

Detailed information concerning this Sandia test may be obtained from the authors.

II. COPCON Model Development

One of the principal purposes of the test described above is to provide a well designed, instrumented, and documented experiment against which existing melt/concrete interaction computer codes may be compared (e.g., BETZ, KAVERN (KWU), COPCON (Sandia), GROWS (ANL), and WECHSL (KFK)).

The COPCON (core/concrete interaction) computer code is being developed at Sandia Laboratories under sponsorship of the Fuel Behavior Research Branch, NRC, as part of the combined experimental/analytical Molten Fuel Concrete Interactions Study. The objective of the modelling effort is to develop and verify a molten fuel/concrete interaction code capable of providing quantitative

estimates of pertinent phenomena, e.g., the nature and rate of gas evolution, and the rate and direction of melt penetration, suitable for risk assessment of light water reactors.

CORCON contains the mass and energy transport and chemical reaction models necessary to describe the interaction process. The principal components of the system are the concrete crucible or container, the molten pool, and the atmosphere above the pool. These are cast in a two-dimensional, axisymmetric geometry as illustrated in the sketch. The initial concrete cavity may be either a flat or hemispherically based right circular cylinder or an arbitrary shape defined in terms of n - r, z body points. Three "default" concrete compositions, specified in terms of 12 species, are included in the code (Table I). These are representative of LWR basaltic aggregate and limestone aggregate concretes, and a generic southeastern United States concrete (the so-called CPRR concrete). The pool is treated as a multi-layered structure ranging from a single one-phase or heterogeneous mixture layer to separate oxidic and metallic layers surmounted by a coolant layer. Each layer is treated as isothermal in bulk (well stirred) and the relative orientation of the layers is determined by the bulk layer densities. The atmosphere above the melt is modelled as an isothermal mixture of reacting gases. The code treats the conservation of mass and energy throughout the system including the interaction with the surroundings. Inter- and intra-component mass and energy transport and generation are described using phenomenological

models obtained from [illegible]ture, the majority of which are based on empirica[illegible]i-empirical correlations. Chemical equilibrium is assumed within each component.

The phenomenological [illegible] having the greatest impact on the interaction process ar[illegible] dealing with heat transfer within the melt and across the melt/concrete interface, concrete erosion and cavity shape change, and melt/gas-phase chemical reactions.

Heat transfer across the pool/concrete interface is described using applicable gas-film models. The Taylor instability model for a horizontal surface is employed along the cavity bottom, up to a local surface inclination angle of 15°, at which point the bubbling of concrete decomposition gases into the pool ceases. At higher surface angles, i.e., around the sides of the pool, laminar and turbulent continuous gas film heat transfer models similar to those developed for film boiling are utilized. When coupled together with appropriate transition regions, these models provide a continuous description of the pool/concrete interface heat transfer around the periphery of the pool.

Heat transfer from the interior of the melt to its pheriphery and across pool layer interfaces is strongly affected by the gas flow into the pool from the decomposing concrete. Enhanced heat transfer as a result of the gas driven circulation may be categorized as either indirect (bubble agitation), for surfaces across which there is no gas flow, e.g., steeply inclined surfaces, or direct (gas injection), for surfaces through which

there is gas flow, e.g., bottom and top of the pool, and layer interfaces. The associated heat transfer coefficients are modelled using empirical correlations for gas driven circulations faired into standard turbulent natural convection correlations as the injected gas flow approaches zero.

Concrete erosion is described using a quasi-steady, one-dimensional ablation model applied at each point on the melt/concrete interface at each time step. Values of the concrete "heat of ablation" required for this model were obtained for the three "default" concretes from experimental investigations of the thermal decomposition behavior of these representative types. The concrete ablation model is coupled to a two-dimensional, axisymmetric shape change procedure which utilizes the local surface recession values to define a new cavity shape at each time step.

Melt/gas-phase chemical reactions are treated thermodynamically for the following two subsystems: gas-metal phases and gas-oxide phases. Each subsystem is assumed to reach chemical equilibrium during each time step, but they are not in equilibrium with one another. The method employed is to minimize the free-energy of a reacting chemical system at constant temperature and pressure subject to the mass balance constraint. This is accomplished using a first order, steepest descent minimization technique. Its main advantages are that neither the reactions nor their order of occurrence need be known and that convergence is guaranteed. The principal disadvantages are that although the solution follows the

phase rule it does not do so completely, and that trace species in the melt are not accurately determined.

The initial version of CORCON is operational and is currently being debugged and checked out on sample problems. A topical report/users manual to describe the content and operation of the code is in preparation. It is anticipated that a draft version of this report will be completed by the end of the calendar year.

The first application of CORCON will be to perform prediction calculations for the Sandia code comparison test. The initial and boundary conditions for this test will be supplied to the various code evaluators during November 1979. Each will be provided the same and sufficient information about the test to facilitate the comparison calculations. The test results will be suppressed until all calculations have been completed. A number of specific interaction phenomena and events are to be predicted. The calculations will be exchanged with other evaluators for analysis and comparison of the computed and experimental results. Finally, these analyses and their results will be documented and distributed.

References:

1) D. A. Powers, D. A. Dahlgren, J. F. Muir and W. D. Murfin "Exploratory Study of Molten Core Material/Concrete Interactions July, 1975 - March 1977," SAND77-2042, Sandia Laboratories, Albuquerque, NM 87185, Feb, 1978.

2) W. B. Murfin, "A Preliminary Model for Core/Concrete Interactions" SAND77-0370, Sandia Laboratories, Albuquerque, NM 87185, Oct., 1977.

3) J. F. Muir "Response of Concrete Exposed to a High Heat Flux on One Surface" SAND77-1467, Sandia Laboratories, Albuquerque, NM 87185, Nov. 1977.

4) D. A. Powers "Sustained Molten Steel/Concrete Interactions Tests" Proceedings, Post Accident Heat Removal Information Exchange Nov. 2-4, 1977, L. Baker, Jr. and J. D. Pingle, eds., ANL-78-10, Argonne National Labs., Argonne, Illinois 60439.

5) D. A. Powers, "Sustained Molten Steel/Concrete Interactions Tests," SAND77-1423, Sandia Laboratories, Albuquerque, NM 87185, June 1978.

6) D. A. Powers "Influence of Gas Generation on Melt/Concrete Interactions" Proceedings of the IAEA International Symposium on the Thermodynamics of Nuclear Materials, Julich, West Germany, IAEA-SM-236/58, IAEA, Vienna, Austria, in press.

7) D. A. Powers "A Survey of Melt Interactions with Core Retention Materials" Proceedings of the International Meeting on Fast Reactor Safety Technology, August 19-23, 1979, Seattle, Washington, in press.

8) R. L. Knight and J. V. Peck, "Model and Computer Code for Energy and Mass Transport in Decomposing Concrete and Related Materials," Proceedings of the International Meeting on Fast Reactor Safety Technology, August 19-23, 1979, Seattle, Washington, in press.

9) D. A. Powers, "Transient Interactions Between Large Steel Melts and Concrete" Sand79- , Sandia Laboratories, Albuquerque, NM 87185, in press.

Table I. Concrete Compositions (weight percent)

Species	Basaltic Concrete	Limestone-Common Sand Concrete	Generic Southeastern United States Concrete
Fe_2O_3	6.25	1.44	1.20
Cr_2O_3	nd	0.014	0.004
MnO	nd	0.03	0.01
TiO_2	1.05	0.18	0.12
K_2O	5.38	1.22	0.68
Na_2O	1.80	0.082	0.078
CaO	8.80	31.2	45.4
MgO	6.15	0.48	5.67
SiO_2	54.73	35.7	3.6
Al_2O_3	8.30	3.6	1.6
CO_2	1.5	22.0	35.7
SO_2	0.2	0.2	nil
H_2O	5.0	4.7	4.1

nd = not determined

Table II

Comparison of Data From Experimental Program with Assumptions in Wash 1400

Phenomenon	Assumption	Observation
I) Melt Behavior		
1) Stratification	No	Yes
2) Agitation	Natural Convection	Vigorous gas-induced forced convection
3) Crust formation	Yes	Oxide layer only
4) Precipitation	Yes	Yes in metal; not observed in silica rich oxides
5) Melt Oxidation	No	Cr and Fe oxidized; Oxidation of Fe and Ni limited by composition of atmospheric gases
II) Thermal Behavior of Concrete		
1) Spallation	Significant first meter	Not significant; only to 3-5 mm.
2) Erosion Rate	180 cm/hr at steady state	Depends on heat flux from melt; 25-135 cm/hr
3) Direction dependence of concrete erosion	two models $h^*/d < 1$ and $\frac{h^*}{d} = 1$	$h^*/d < 1$; depends on melt geometry and gas generation rate.
4) Heat disposition	All into concrete	Depends on gas generation rate; 21 to 32% into concrete.
5) Reinforcing steel	No significant effect	No significant effect
6) Water migration	Not considered	Both away from and into hot zone.
7) Concrete melting	2200°C melting point	Melting range depends on concrete composition solidus ~ 1100°C; liquidus ~ 1400 to 1600°C.
8) Decomposition	Thermodynamically controlled dehydration 500°C decarboxylation 770-89°C	Kinetically controlled; depends on temperature heating rate and atmosphere composition dehydration 25-500°C decarboxylation 550-1000°
9) Concrete cracking	Not considered	Fracture induced by tensile, thermal stresses

Phenomenon	Assumption	Observation
III) Gas Production		
1) CO_2 and H_2O	Composition and amount proportional to concrete eroded	Neither composition or amount proportional to concrete eroded: depends on heat transfer in concrete.
2) CO and H_2	No; gases assumed to bypass melt	Yes; CO_2 and H_2O reduced as they percolate through melt; gas composition controlled by Fe/FeO equilibrium.
3) Hydrocarbons	No	Hydrogenation of CO observed to yield methane, ethene, and ethane. Hydrogenation maybe catalyzed by heated structures near interaction zone.
4) Gas ignition	No; flammability limits of well-mixed gas	Observed when oxygen available and gases hotter than 500°C. Diffusional flame limits may be applicable.
IV) Aerosols		
1) Generation	Yes	Yes; multimodal mean sizes < 1 μ and < 5 μ.
2) Amount		Depends on melt temperature and gas generation rates; 35 to 150 g/m^3.
3) Composition	Only radioactive aerosols considered	Significant non-radioactive component 10% - 35%.

TABLE III

DATA NOW AVAILABLE

Gas Generation Rates

Gas Composition

Melt Penetration

Heat Flux Partitioning

Aerosol Formation

Melt Chemistry

Fission Product Chemistry

Chemistry and Thermal Behavior of Concrete

Table IV. Kinetic Parameters for Concrete Decomposition*,≠

Reaction	Basaltic Concrete	Limestone-Common Sand Concrete	Generic Southeastern United States Concrete
loss of evaporable water (n=1)	$E = 11.6$ $K = 4.4 \times 10^{6}$	$E = 11.0$ $K = 1.29 \times 10^{6}$	$E = 11.0$ $K = 1.29 \times 10^{6}$
loss of chemical water (n=1)	$E = 41.9$ $K = 2.8 \times 10^{12}$	$E = 40.8$ $K = 1.96 \times 10^{12}$	$E = 40.8$ $K = 1.96 \times 10^{12}$
decarboxylation (n=1)	$E = 42.6$ $K = 3.6 \times 10^{9}$	$E = 38.5$ $K = 1.98 \times 10^{7}$	$E = 45.8$ $K = 1.73 \times 10^{9}$
decarboxylation (n=2/3)	--- ---	$E = 37.0$ $K = 3.6 \times 10^{7}$	$E = 44.9$ $K = 1.94 \times 10^{6}$

*E in units of Kcal/mole; K in units of minutes^{-1}

≠Standard errors in E ~ 10%; standard errors in K ~ 30 to 50%

Table V. Aerosol Compositions

Element	NSS-1 ppm wt.	NSS-3 ppm wt.	
U	550	3100	
Al	>1%	1300	
Zr	3	70	
Fe	>1%	>1%	melt constituents
Cr	750	>1%	
Mn	>1%	2500	
Ce	31	31	
La	93	82	
Sr	250	110	fission product mocks
Cs	>0.5%	>0.5%	
Sn	>1%	>1%	
Mo	1%	>0.5%	
Mg	540	1900	
Ca	310	290	
P	1%	2400	concrete materials
Na	3200	0.5%	
Si	>1%	>1%	
F	>1%	>1%	
Cl	1900	3	
S	>1%	>1%	
Hf	9.9	3.9	
W	1.6	380	
Lu	0.66	0.66	impurities in fission product mocks and melt materials
Yb	0.9	2.0	
Tm	0.95	0.37	
Eb	1.1	0.83	
Ho	0.61	0.61	
Dy	0.38	0.11	
Tb	1.4	1.4	
Gd	3.2	1.3	
Eu	1.2	1.2	
Sm	3.3	3.3	
Nd	51	26	
Pr	1.3	18	
Ba	170	37	
I	62	1400	
Sb	180	>0.5%	
Nb	64	8.5	
Yt	0.46	3.1	
Rb	1100	1100	
As	310	41	

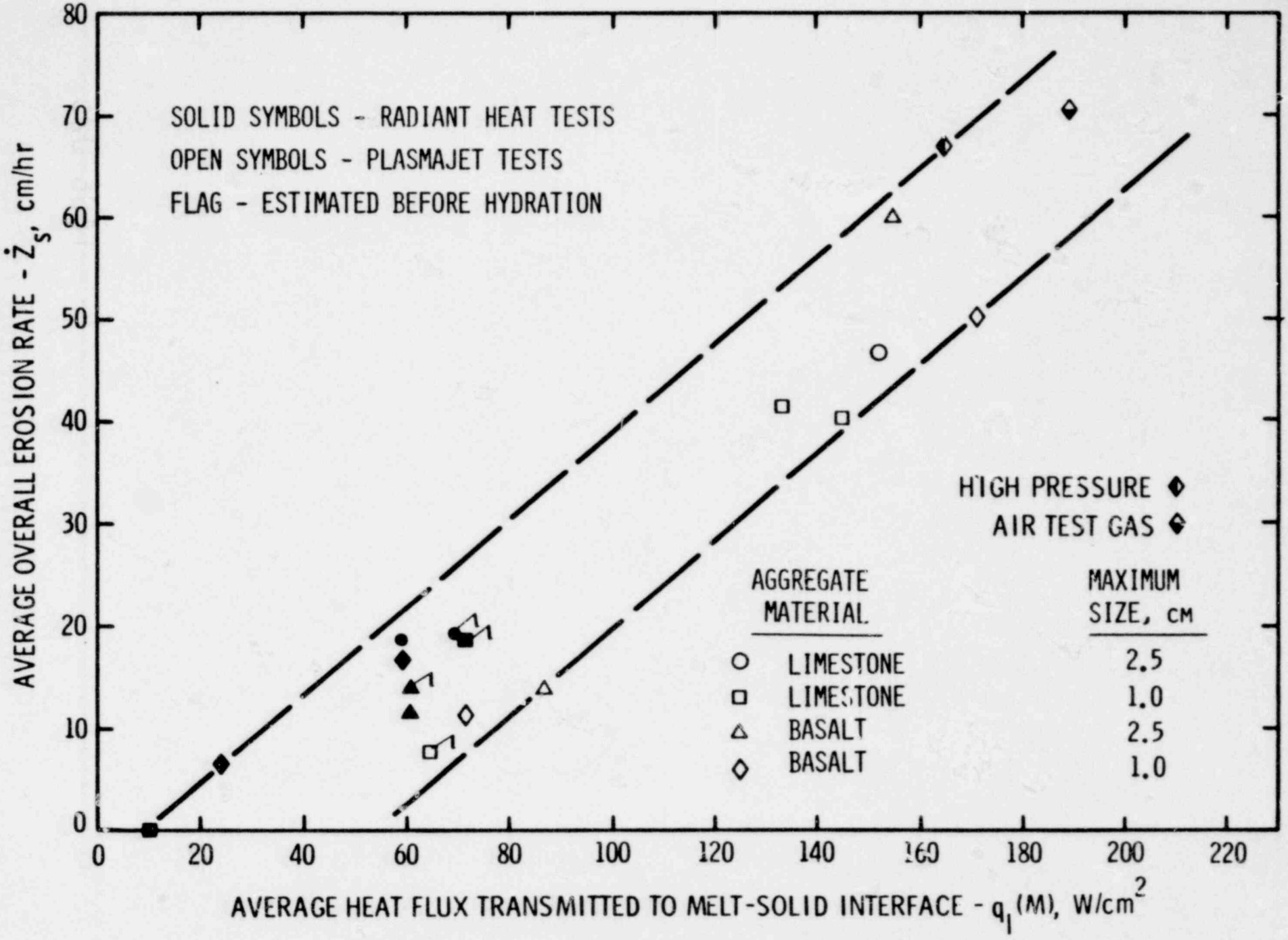

FIGURE 1. VARIATION OF AVERAGE OVERALL EROSION RATES WITH NET HEAT FLUX

FIGURE 2. EFFECT OF TEMPERATURE DIFFERENCE ON THE CONCRETE EROSION RATE

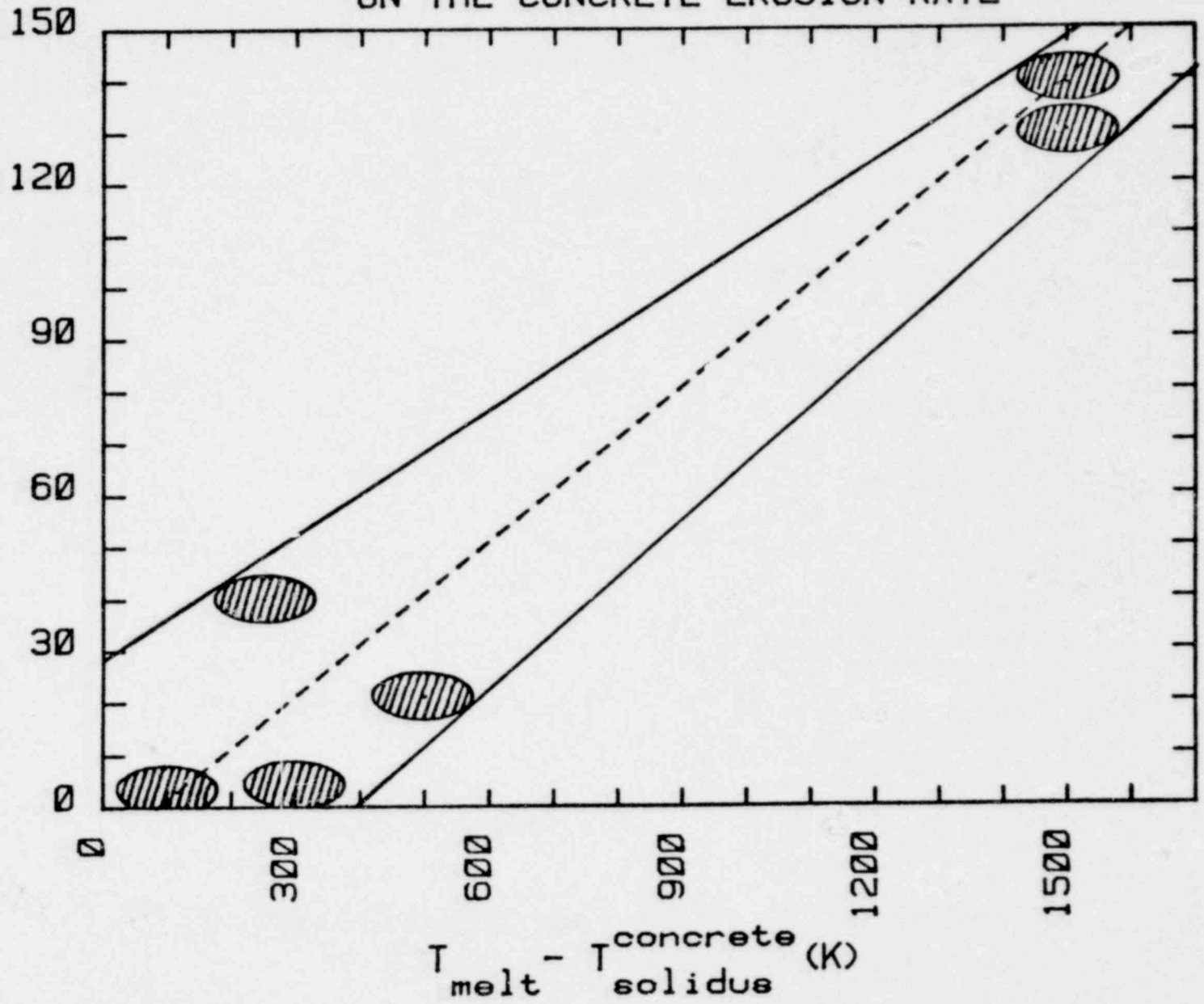

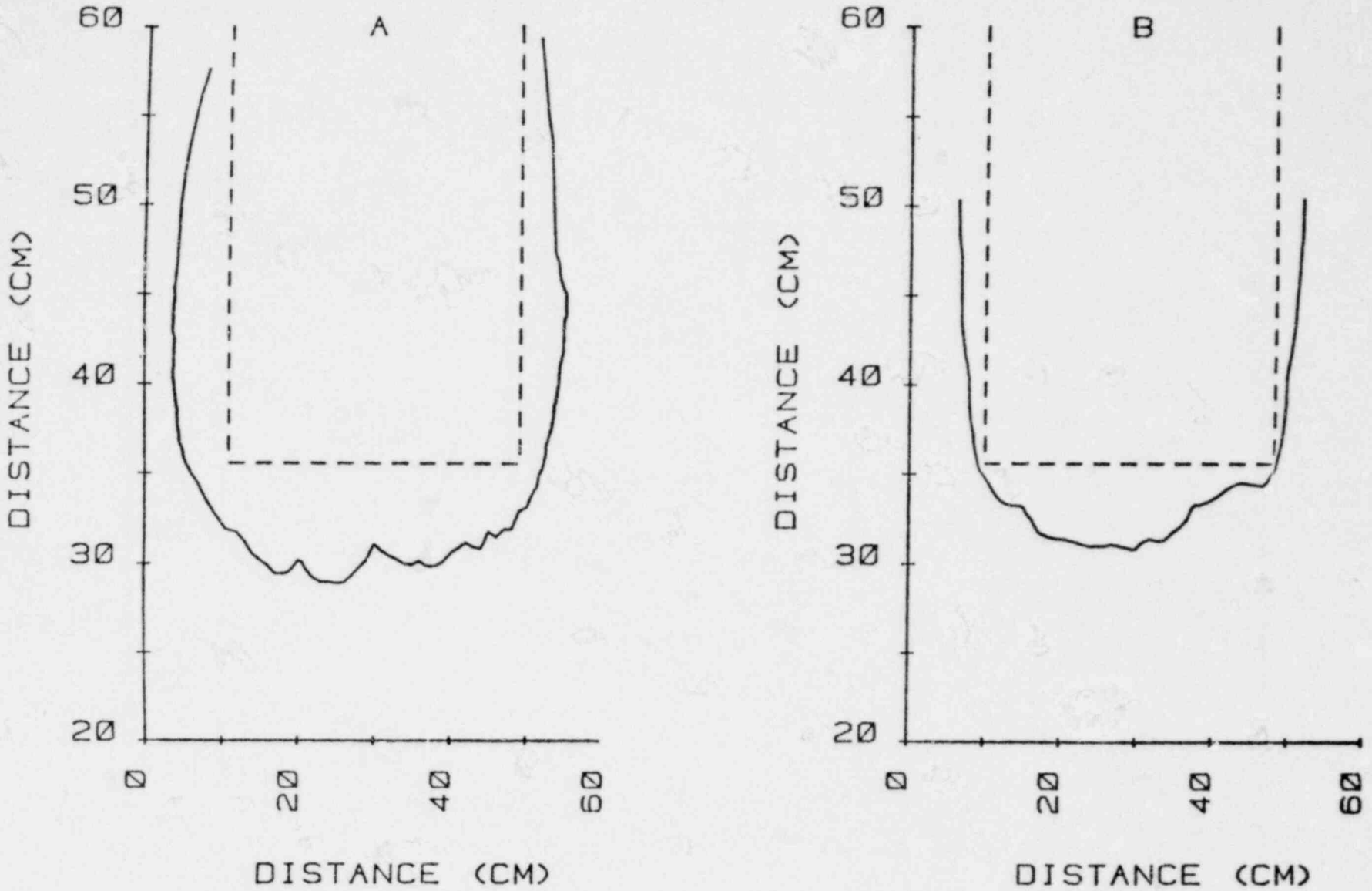

Figure 3. Post-test erosion profiles of A) basaltic concrete and B) generic Southeastern United States concrete crucible after exposure to 1700°C stainless steel. The solid lines are the post-test profiles, and the dashed lines are the original cavity shapes.

FIGURE 4. EFFECT OF GAS VELOCITY ON THE OBSERVED DEPTH OF A SHALLOW POOL

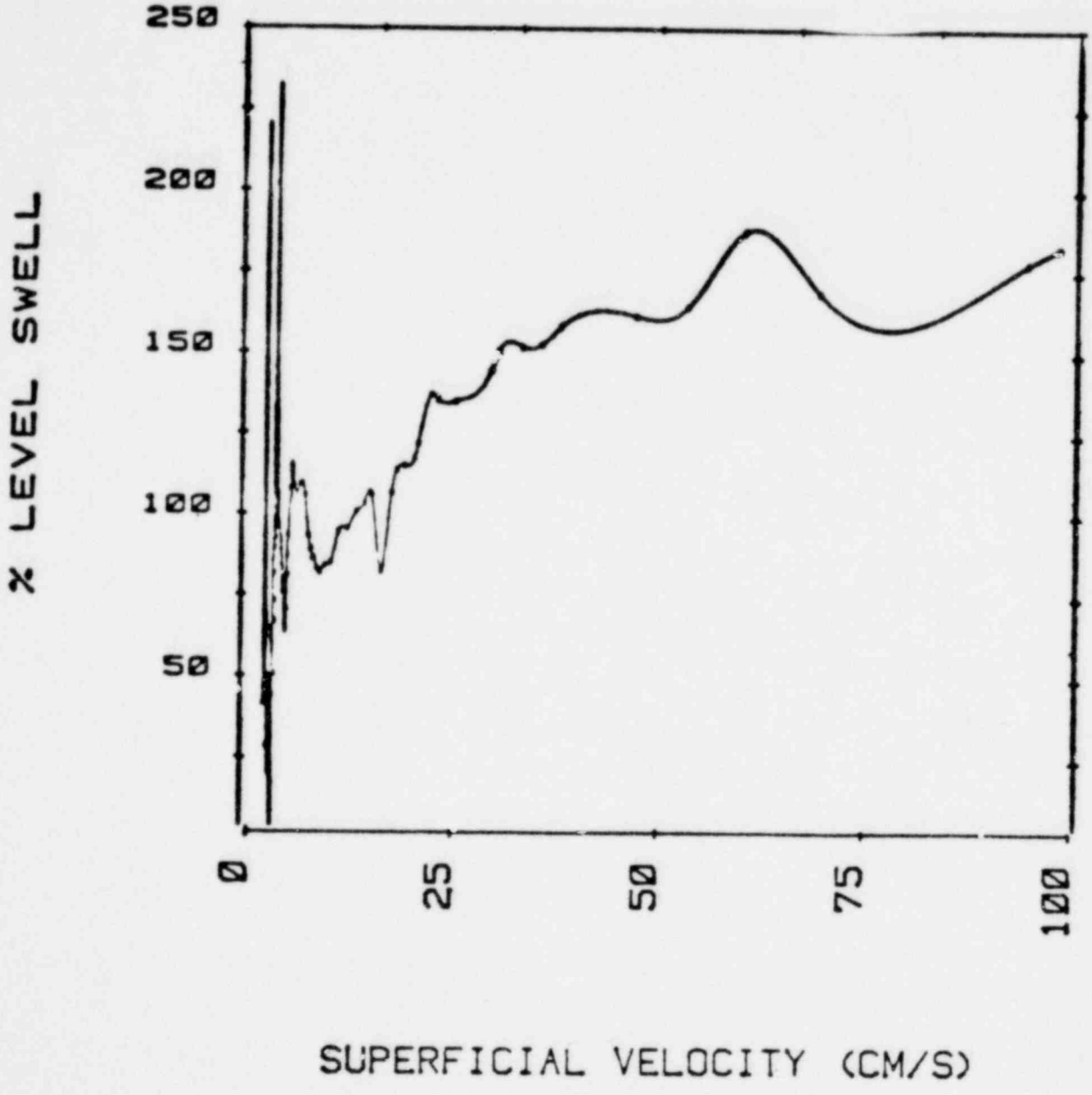

FIGURE 5. OXYGEN FUGACITY OF GAS SAMPLES (points) AND THE Fe-Fe(II)O PHASE BOUNDARY (solid line)

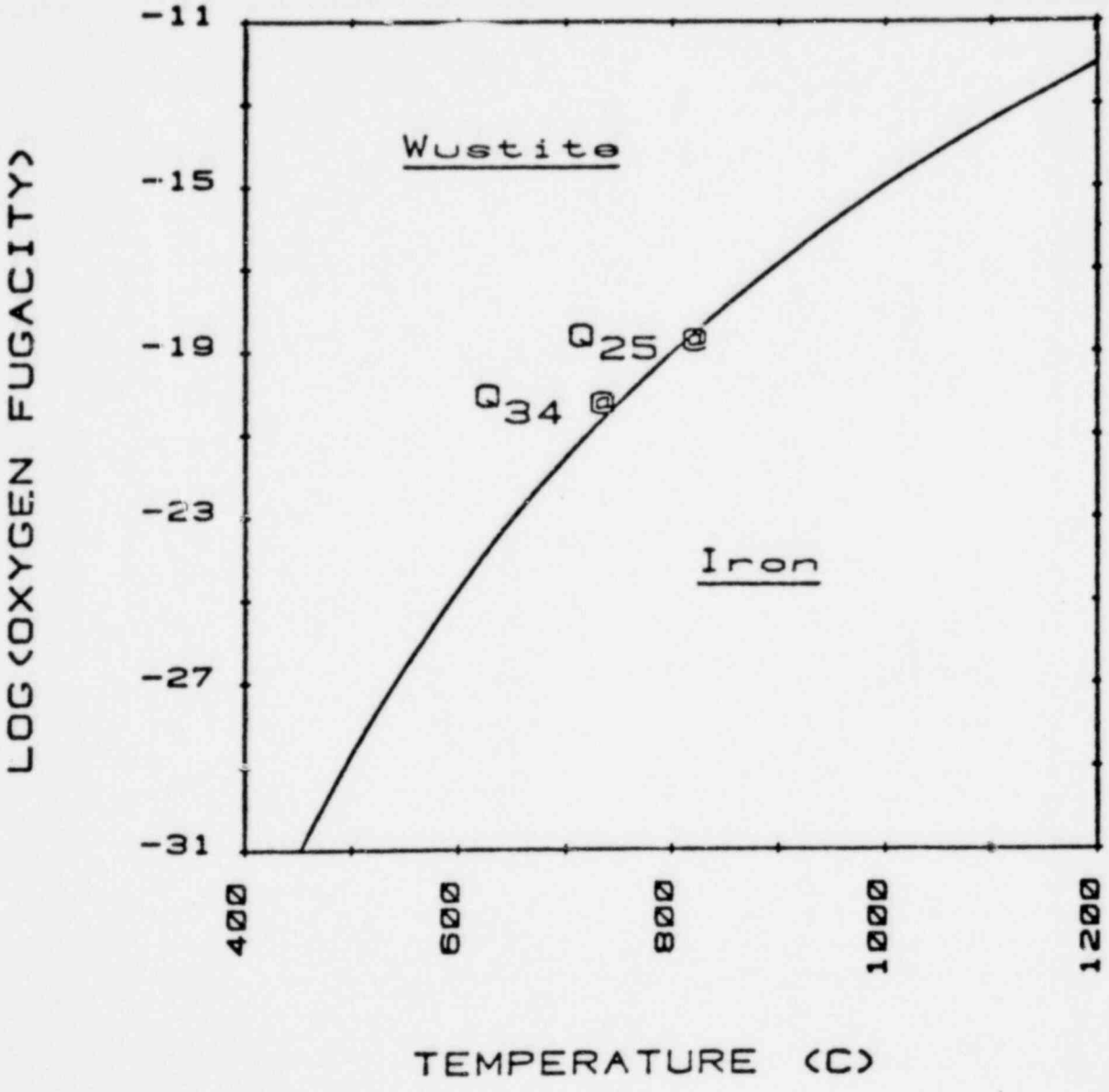

FIGURE 6. METHANE AND HYDROGEN CONTENTS VERSUS GAS TEMPERATURE

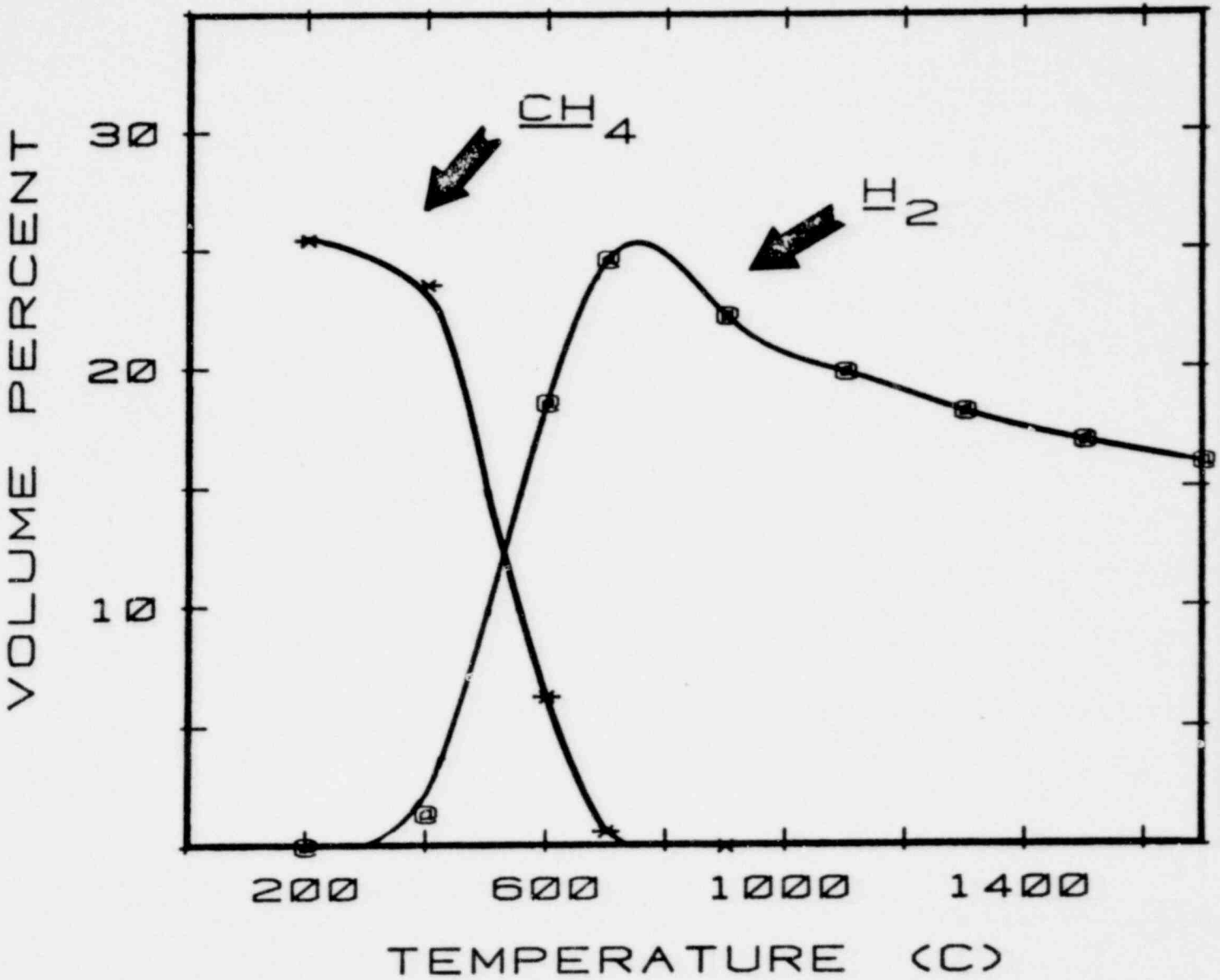

FIGURE 7. AEROSOL CONCENTRATION DURING TRANSIENT CORIUM/CONCRETE INTERACTION

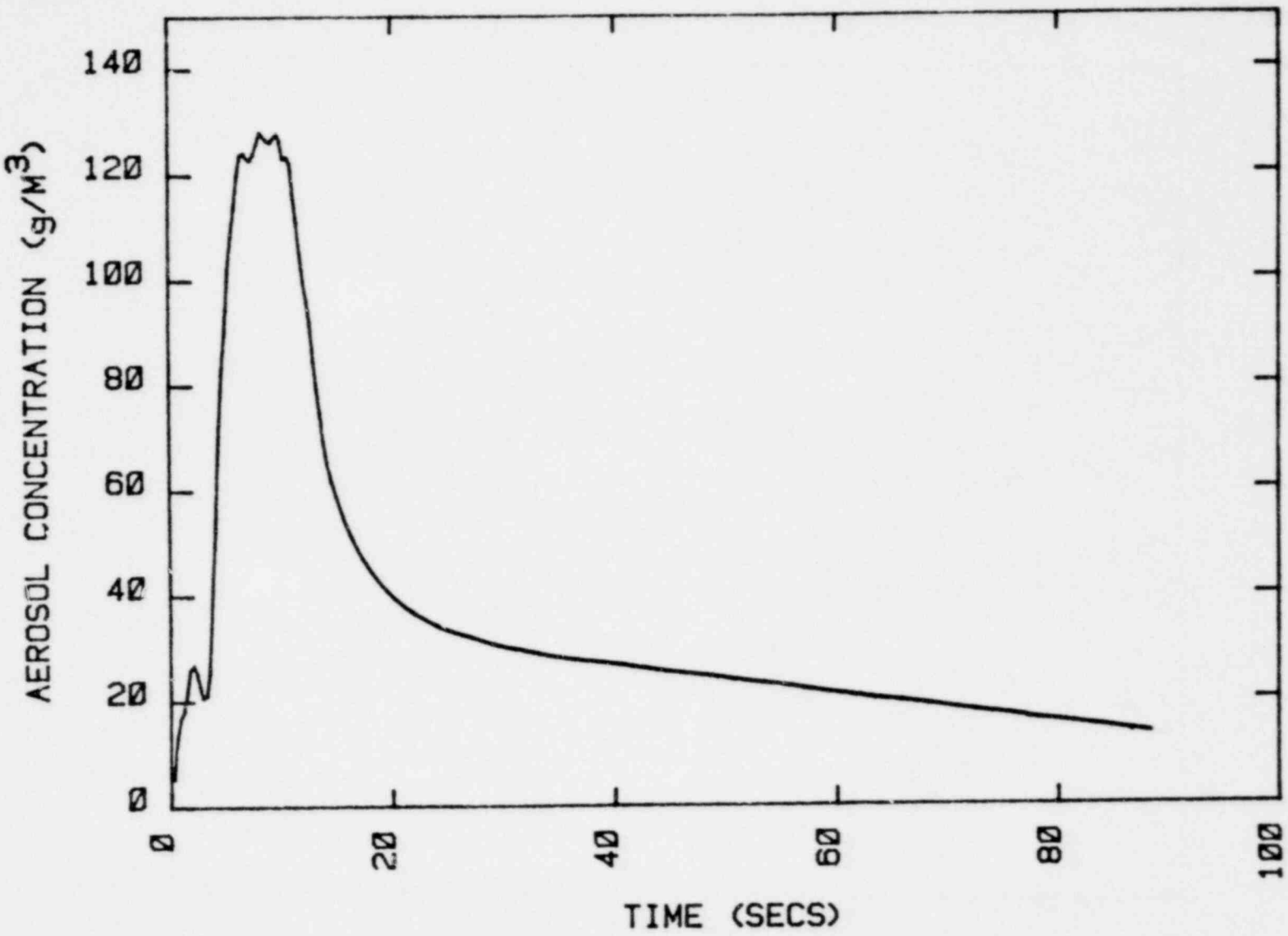

FIGURE 8. PARTICLE SIZE DISTRIBUTION OF AEROSOLS PRODUCED BY MELT ITERATIONS WITH CONCRETE

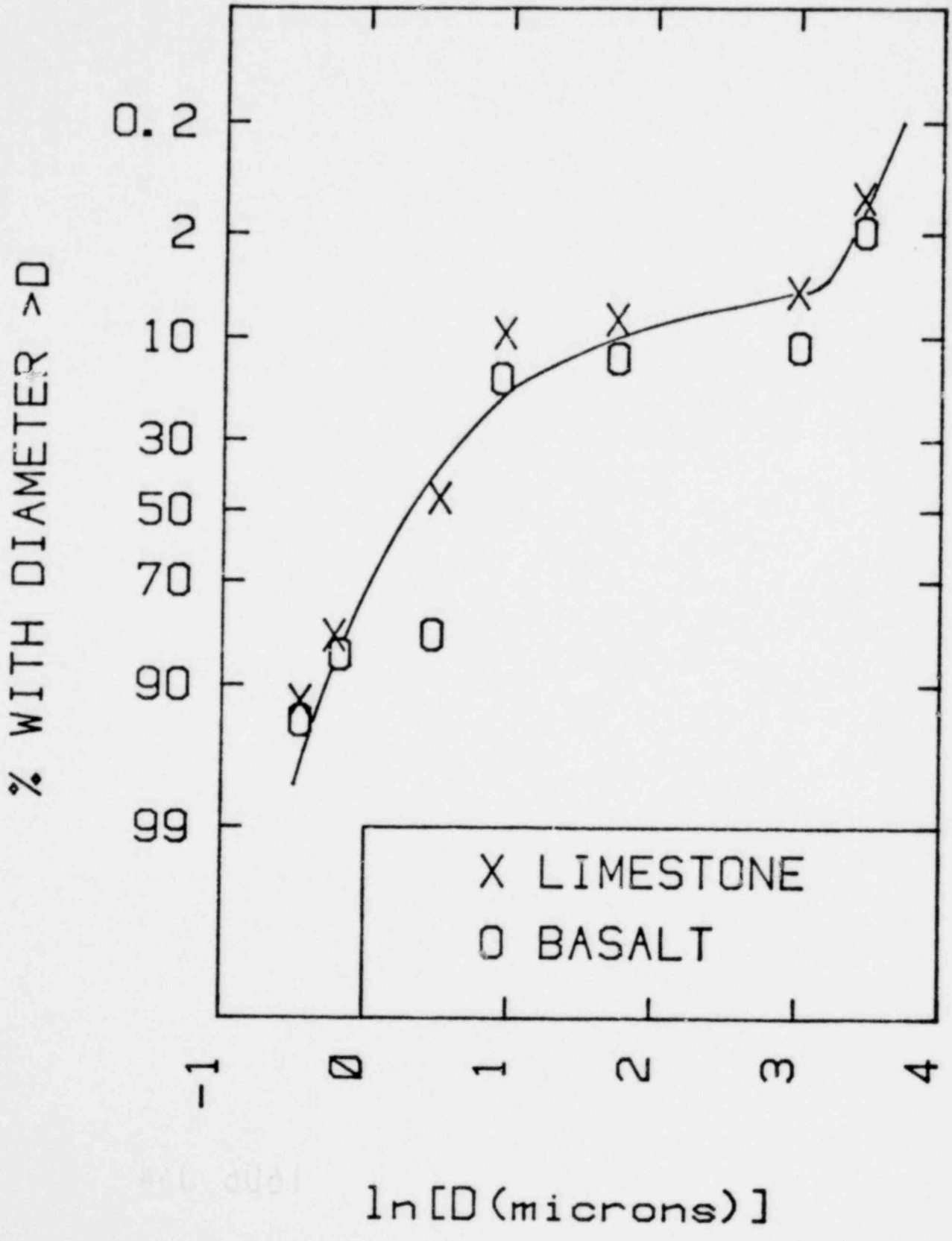

FIGURE 9. EFFECT OF GAS VELOCITY ON THE AEROSOL CONCENTRATION IN THE GAS

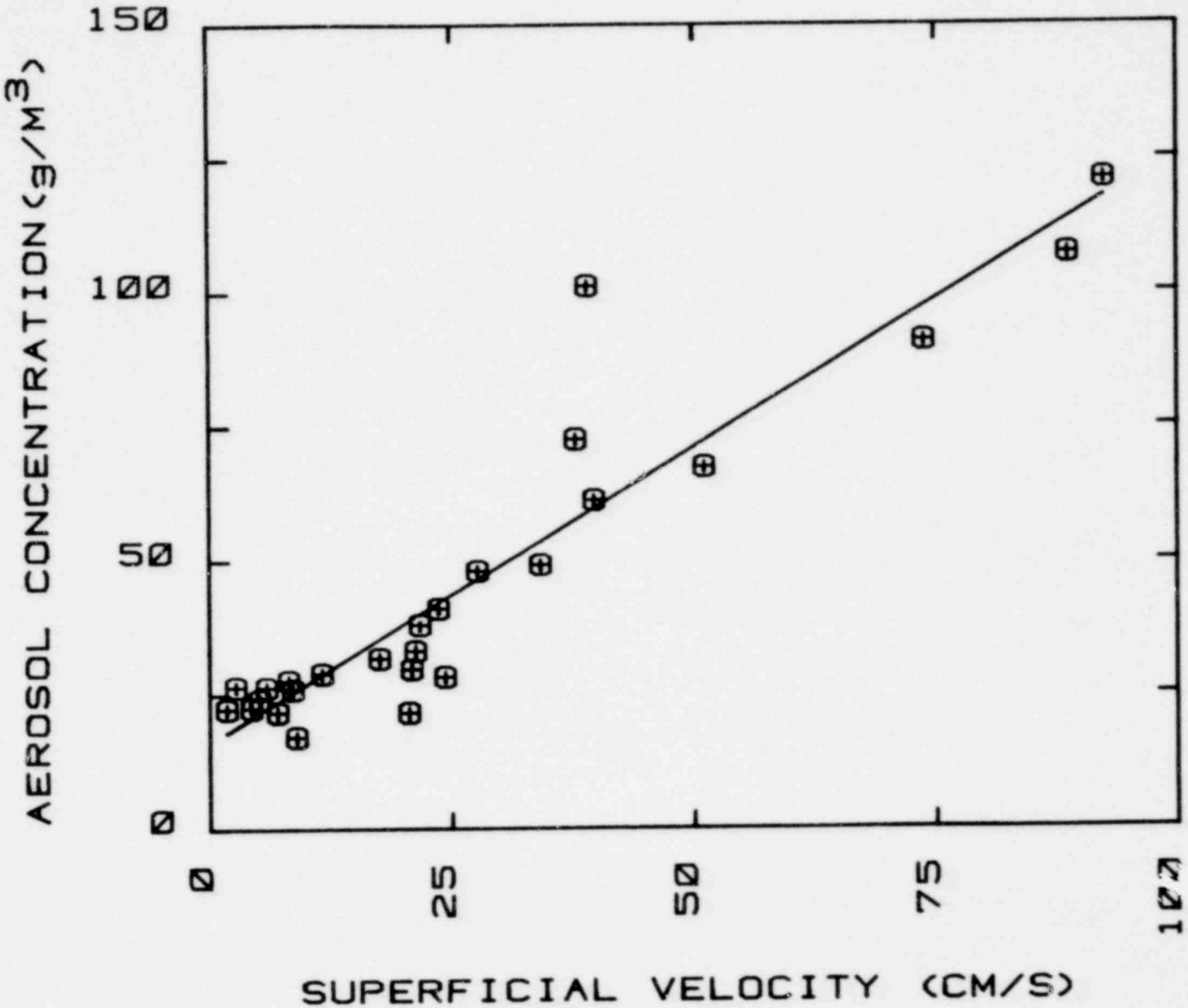

FIGURE 10. SCHEMATIC DEPICTION OF THE TEST PROCEDURE USED FOR THE CODE COMPARISON TEST

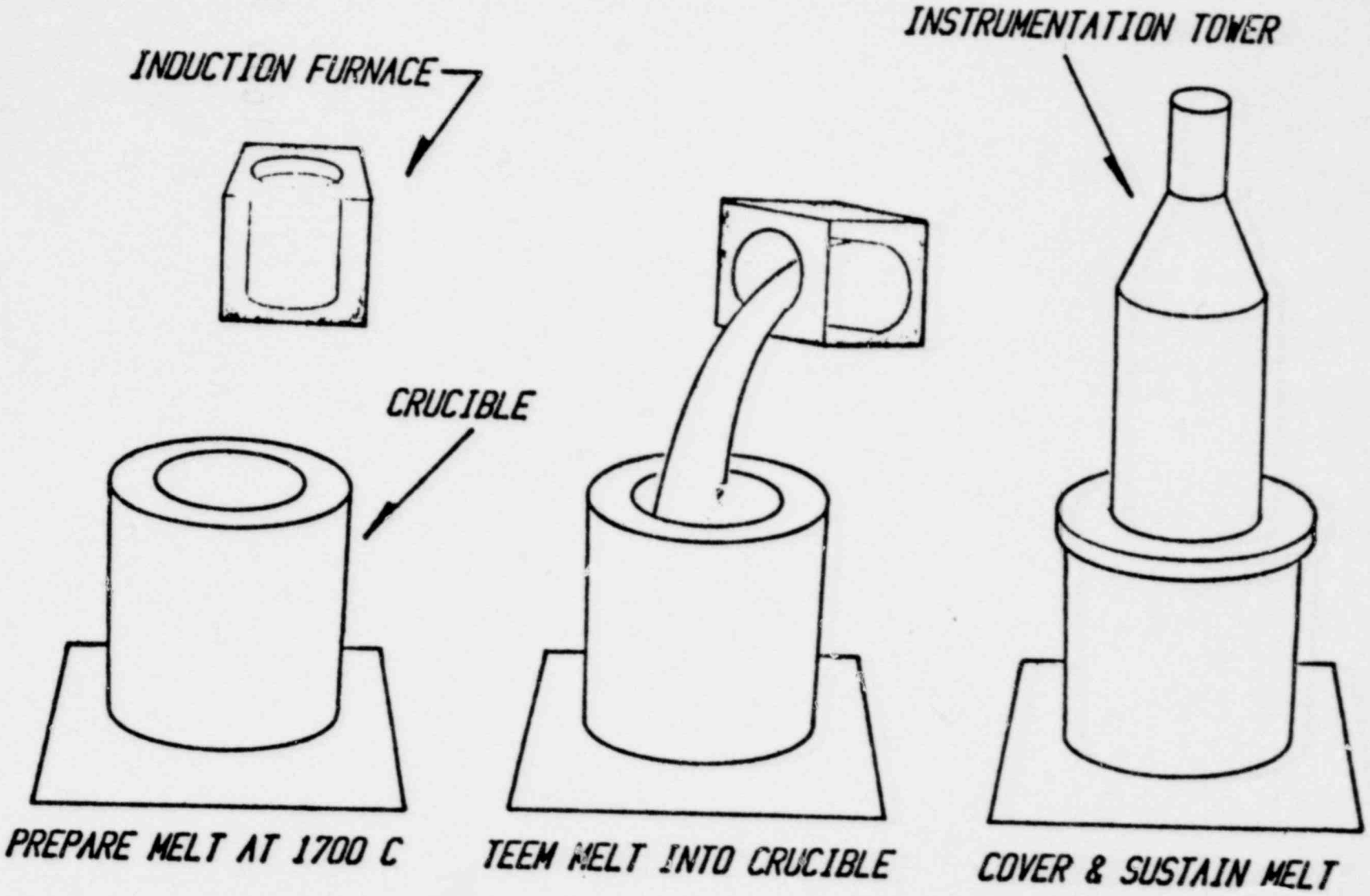

1606 035

CORE/CONCRETE INTERACTION MODEL

CORCON

PRINCIPAL FEATURES

MAIN PHENOMENOLOGICAL MODELS

CODE COMPARISON TEST ANALYSIS

CORCON - PRINCIPAL FEATURES I

GEOMETRY - 2-D, AXISYMMETRIC

MULTILAYERED POOL - 1 TO 4 LAYERS

- ISOTHERMAL CORE

MELT ATMOSPHERE - ISOTHERMAL, REACTING GAS MIXTURE

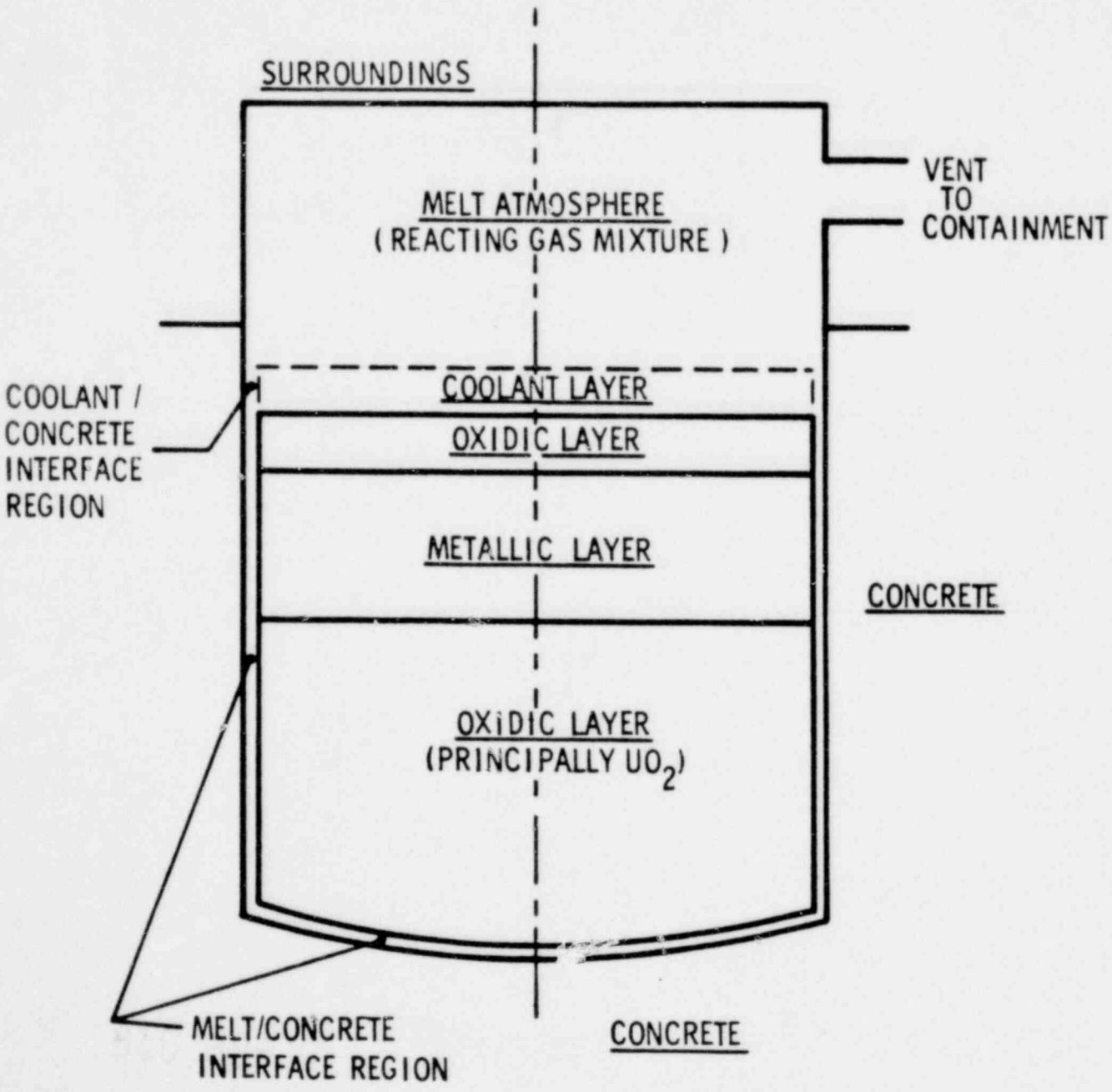

CORCON - PRINCIPAL FEATURES II

INSTANTANEOUS DEPOSITION OF MELT INTO CAVITY

MELT/CONCRETE INTERFACE -

- FLOW CONFIGURATION } VARIABLE AROUND POOL
- HEAT AND MASS TRANSFER } VARIABLE AROUND POOL

MASS AND ENERGY CONSERVATION -

- TRANSPORT - MELT/CONCRETE INTERFACE
  - BETWEEN POOL LAYERS
  - FROM POOL SURFACE - ATMOSPHERE
    - SURROUNDINGS
  - ATMOSPHERE TO SURROUNDINGS
  - VENTING TO CONTAINMENT
- SOURCES/ SINKS
  - CONCRETE DECOMPOSITION
  - CHEMICAL REATIONS
  - FISSION PRODUCT DECAY HEAT
  - ABLATION OF SURROUNDINGS

CONCRETE EROSION - 1-D, STEADY-STATE ABLATION
- 2-D, AXISYMMETRIC CAVITY
- CONCRETE DECOMPOSITION DATA

CHEMICAL REACTIONS - OXIDATION - METALLIC LAYER
- REDUCTION - OXIDIC LAYER
- EQUILIBRIUM - GAS PHASE

IMPROVED MATERIAL PROPERTY DATA

POOL VOID FRACTION AND LEVEL SWELL

IMPROVED NUMERICAL TECHNIQUES

INTERFACE HEAT TRANSFER

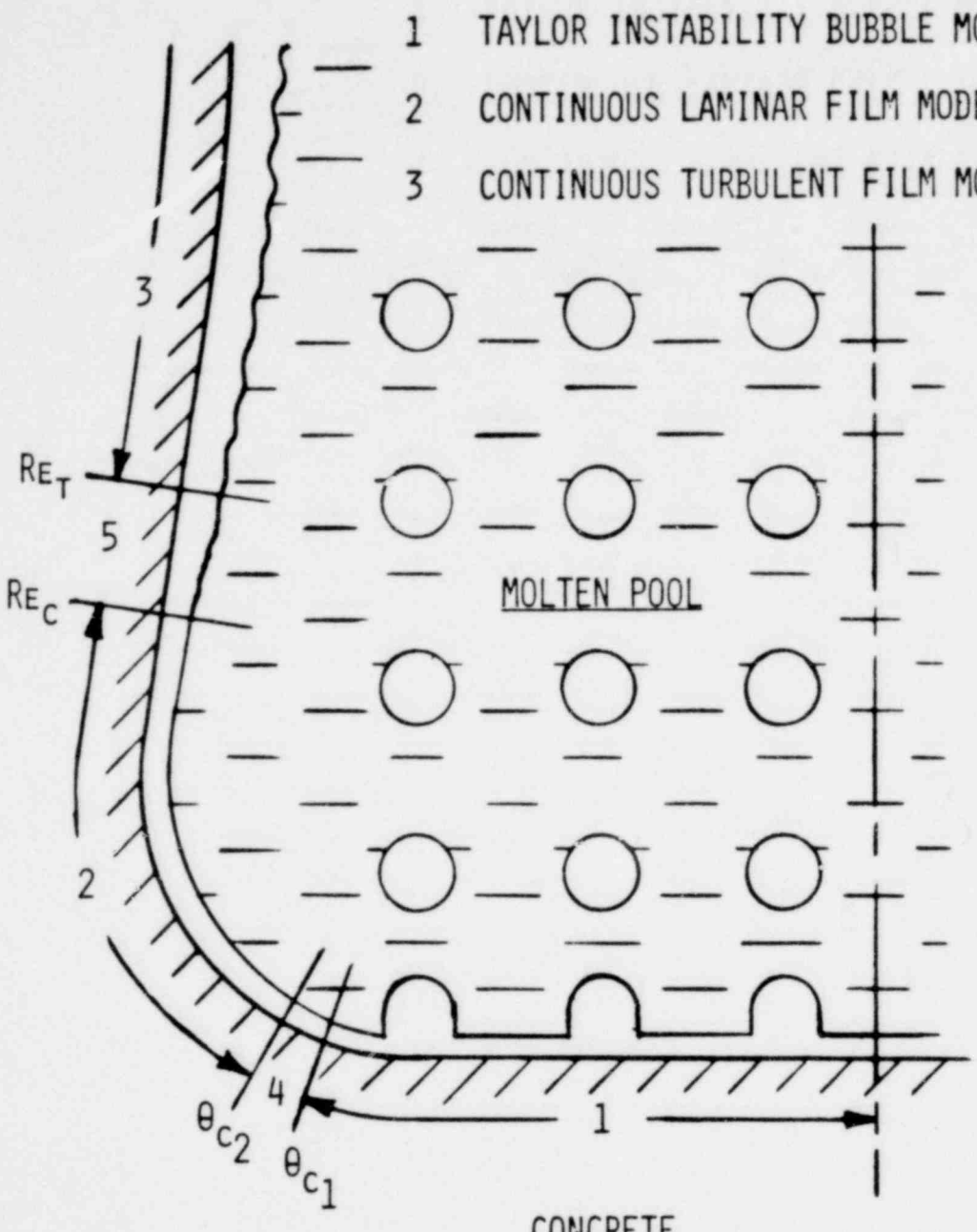

4 TRANSITION REGION, $\theta_{c_1} - \theta_{c_2}$, FROM BUBBLE TO LAMINAR FILM MODEL

5 TRANSITION REGION, $Re_C - Re_T$, FROM LAMINAR TO TURBULENT FILM

INTERFACE HEAT TRANSFER MODELS

1. TAYLOR INSTABILITY MODEL: (BUBBLE MODEL) $Nu_B = 0.326\ Re^{1/3}$

$$Nu_B = \frac{HL'}{K_G} \qquad Re = \frac{\rho_G V_O A}{\mu_G}$$

$$L' = \left[\frac{\mu_G^2}{G\rho_G(\rho_\ell - \rho_G)}\right]^{1/3} \qquad A = \left[\frac{\sigma}{G(\rho_\ell - \rho_G)}\right]^{1/2}$$

LAPLACE CONSTANT

2. LAMINAR FILM MODEL: $Nu_L = 0.563\ Re^{-1/3}$

3. TURBULENT FILM MODEL: $Nu_T = 0.0902\ Pr^{1/3} Re^{1/6}$

$$Nu_{L,T} = \frac{HL''}{K_G} \qquad Re = \frac{\rho_G \bar{U}\delta}{\mu_G}$$

$$L'' = \left[\frac{\mu_G^2}{G\rho_G \sin\theta(\rho_\ell - \rho_G)}\right]^{1/3} \qquad Pr = \frac{\mu_G\ \rho_G}{K_G}$$

$$\bar{U}\delta = \frac{1}{R}\int_0^X RV_O\, d\zeta$$

1606 040

x = STREAMLENGTH

TRANSITION REGIONS

4 BUBBLE TO LAMINAR TRANSITION:

- LINEARIZATION OF HEAT TRANSFER COEFFICIENT ALONG STREAMLENGTH FROM $\theta_{c_1} = 15^o$ TO $\theta_{c_2} = 30^o$

5 LAMINAR TO TURBULENT TRANSITION:

- $Re_c = 100$
- "PERSH" TYPE TRANSITION

$$Nu = Nu_T - \frac{\left(Nu_T - Nu_L\right)_c}{\left(Re/Re_c\right)^2}$$

$$= Nu_T - \frac{\text{CONSTANT}}{Re^2}$$

1606 01

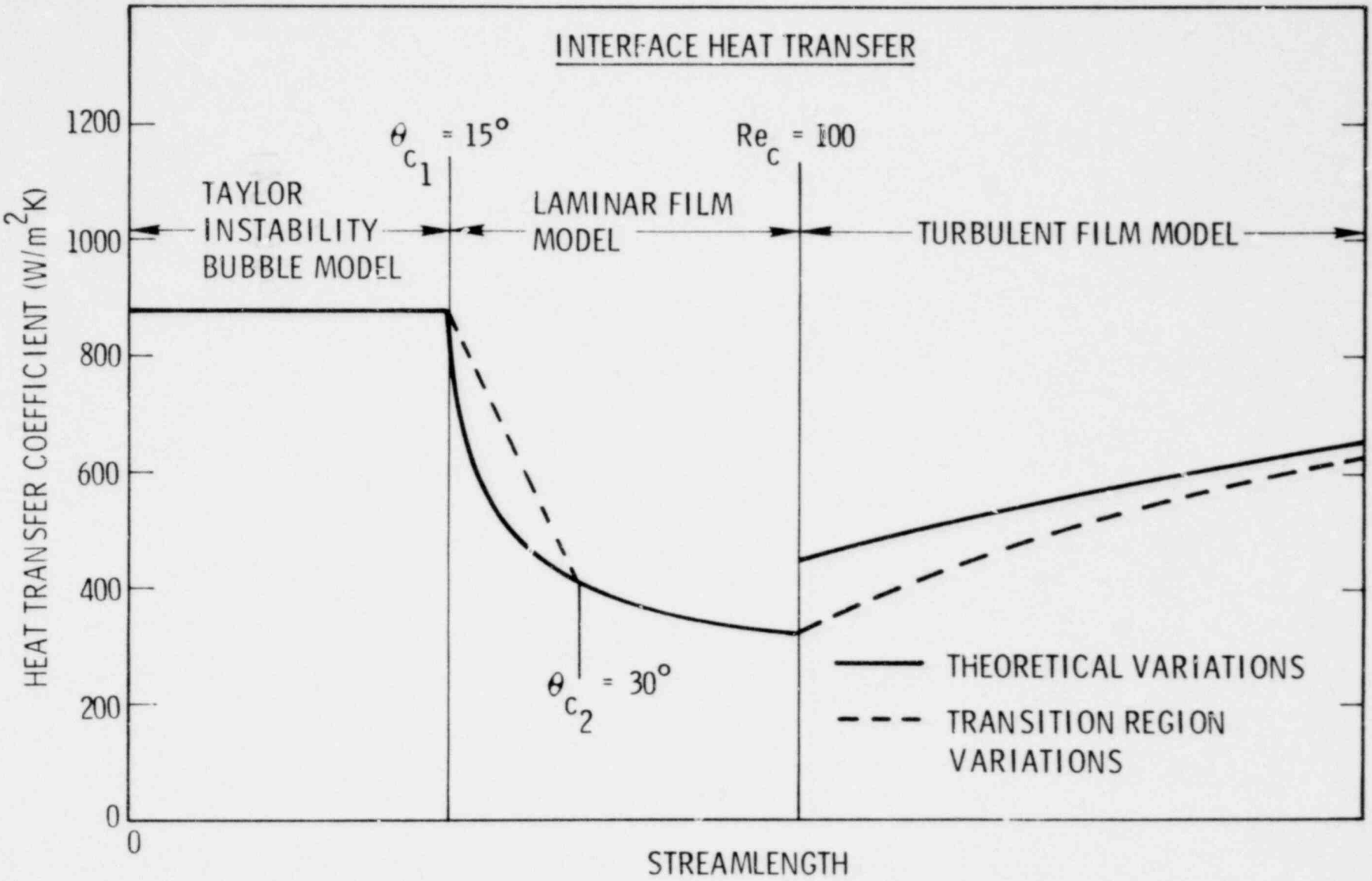
INTERFACE HEAT TRANSFER
1200
1000
800
600
400
200
0
0
HEAT TRANSFER COEFFICIENT (W/m²K)
θc1 = 15°
Rec = 100
TAYLOR INSTABILITY BUBBLE MODEL
LAMINAR FILM MODEL
TURBULENT FILM MODEL
θc2 = 30°
THEORETICAL VARIATIONS
TRANSITION REGION VARIATIONS
STREAMLENGTH

POOL/INTERFACE HEAT TRANSFER

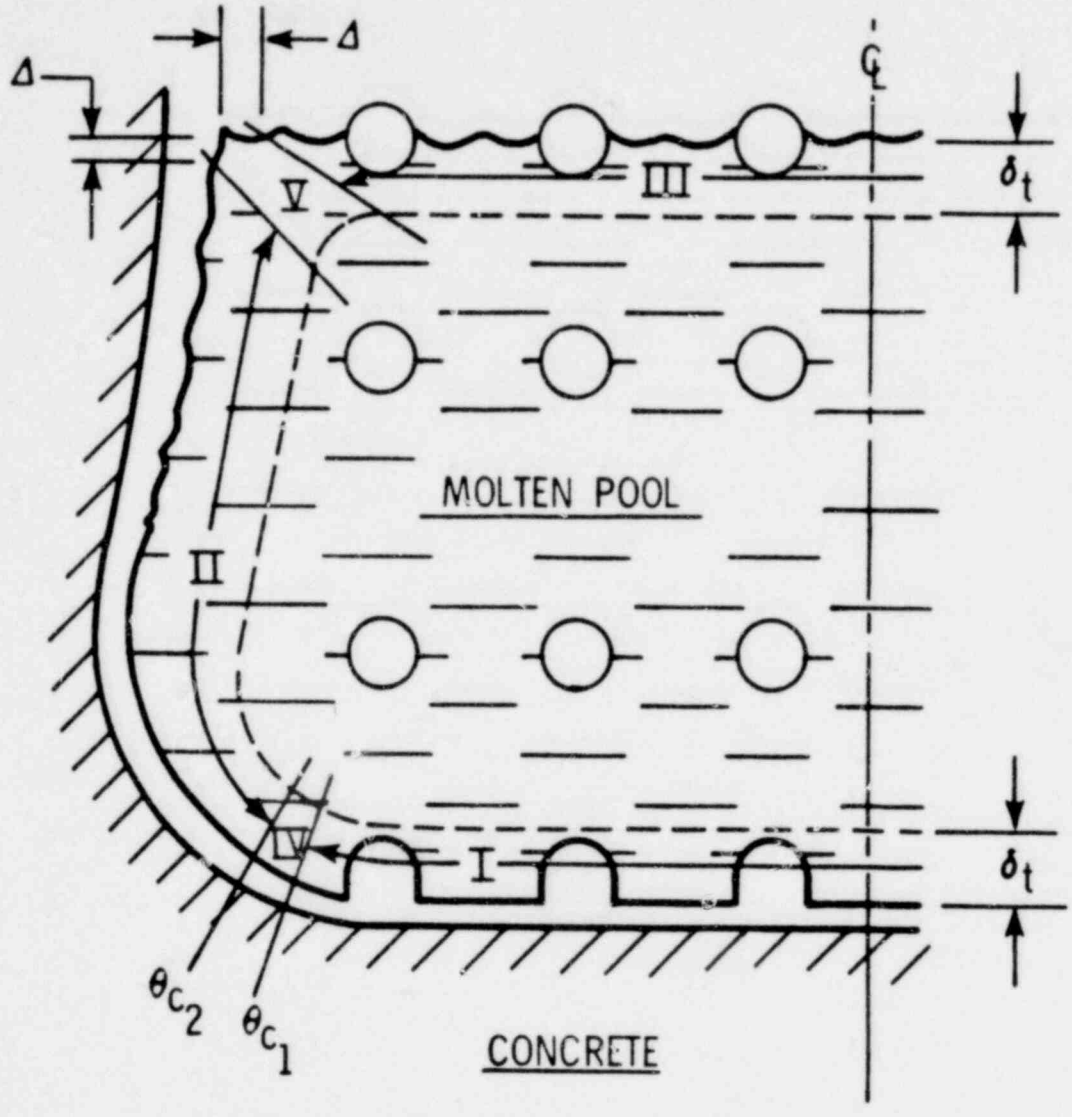

REGION	CONDITION
I, III	SURFACE WITH GAS INJECTION
II	SURFACE WITH BUBBLE AGITATION
IV, V	TRANSITION REGIONS

- GAS DRIVEN CIRCULATION -

- SURFACE WITH BUBBLE AGITATION - II

- BASED ON CORRELATION DEVELOPED BY KONSETOV

- COMBINED WITH TURBULENT NATURAL CONVECTION RELATION

$$H = K\left(Pr\,\frac{G}{\nu^2}\right)^{1/3}(0.00274\,\beta\Delta T + 0.05\,\alpha)^{1/3} \qquad (26)$$

- SURFACE WITH GAS INJECTION - I

- BASED ON CORRELATION DEVELOPED BY GREIF

- COMBINED WITH TURBULENT NATURAL CONVECTION RELATION FOR COOLED HORIZONTAL SURFACE

$$H = K\left(Pr\,\frac{G}{\nu^2}\right)^{1/3}\left(0.00131\beta\Delta T + 0.4\alpha^2\right)^{1/3} \qquad (27A)$$

$$\alpha = \frac{B}{1+B} \quad , \quad B = 0.65V_S\sqrt{GA}$$

HEAT TRANSFER FOR SURFACES
WITH BUBBLE AGITATION

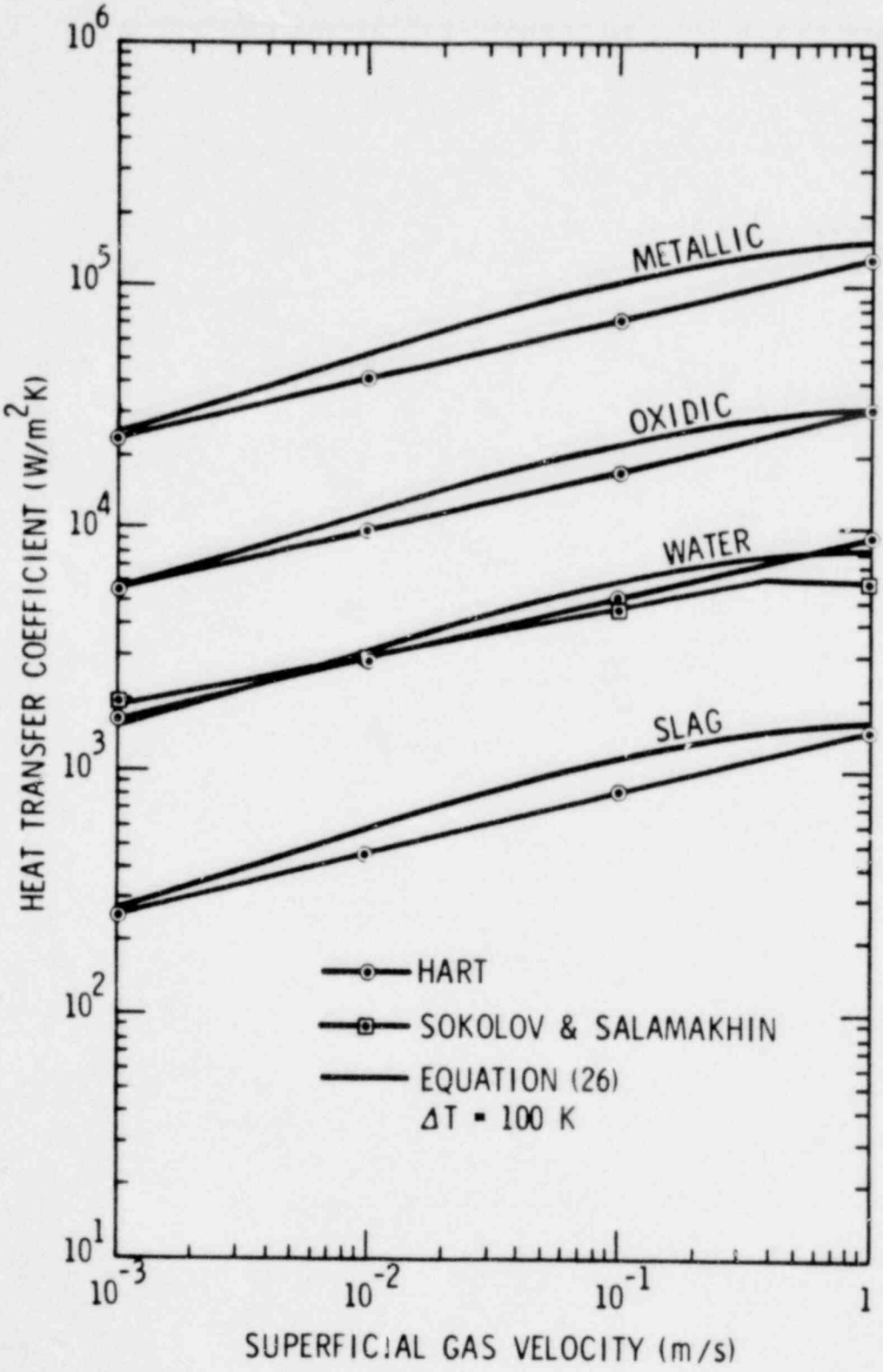

HEAT TRANSFER FOR SURFACES
WITH GAS INJECTION

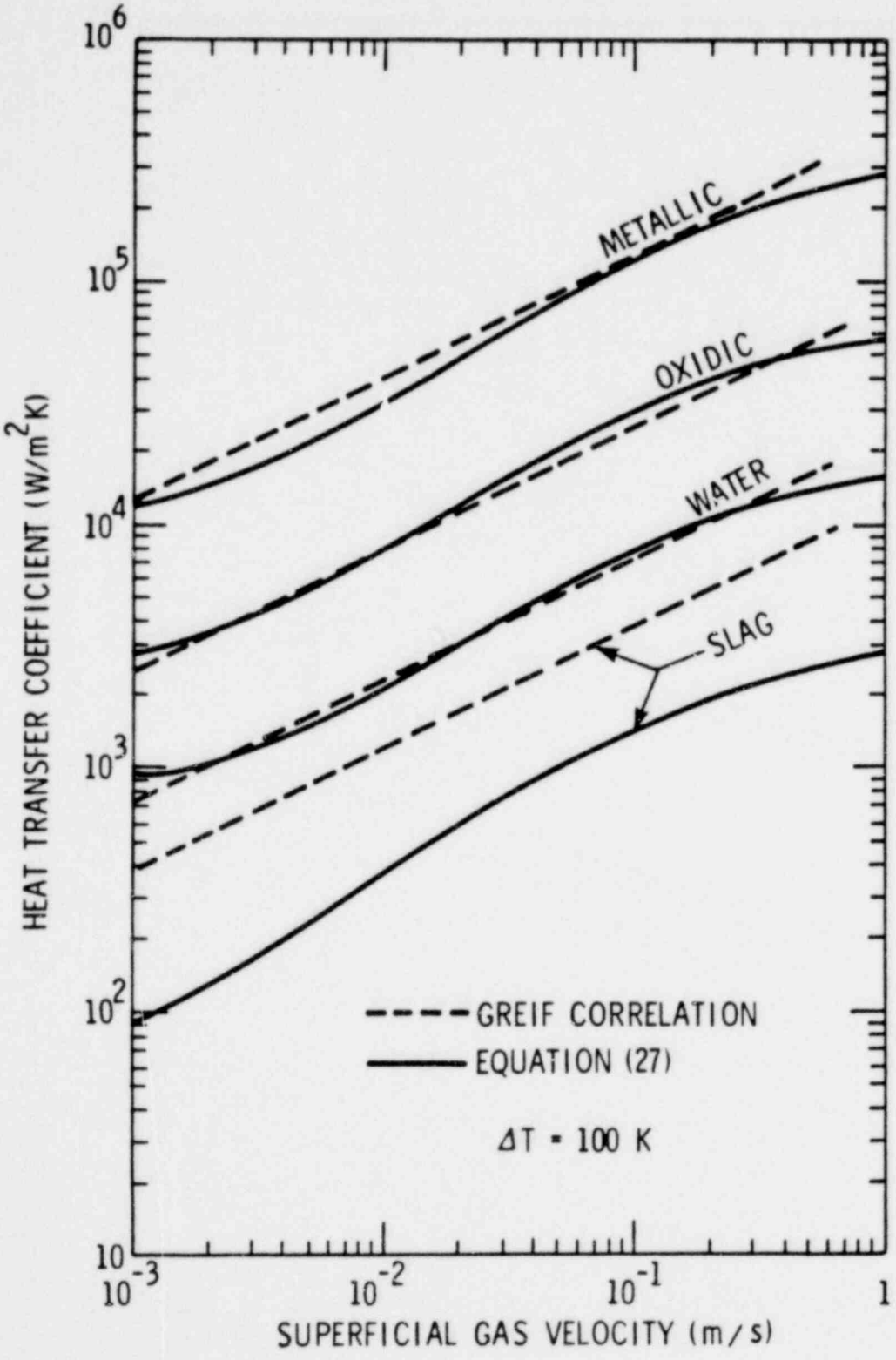

- LIQUID/LIQUID INTERFACES - III

- UPPER LAYER: $H_U = \dfrac{Q}{(T_U - T_I)}$

- LOWER LAYER: $H_L = \dfrac{Q}{(T_I - T_L)}$

- INTERFACE TEMPERATURE: $T_I = \dfrac{H_L T_L + H_U T_U}{H_L + H_U}$

- KONSETOV RELATION MODIFIED TO ACCOUNT FOR INTERFACE DYNAMICS:

$$H_{U,L} = K\left(Pr\,\frac{G}{\nu^2}\right)^{1/3}\left(0.00274\,\beta\Delta T + 50\,\alpha^2\right)^{1/3} \qquad (27B)$$

LIQUID/LIQUID INTERFACE

WITH BUBBLE AGITATION

SLAG-METAL

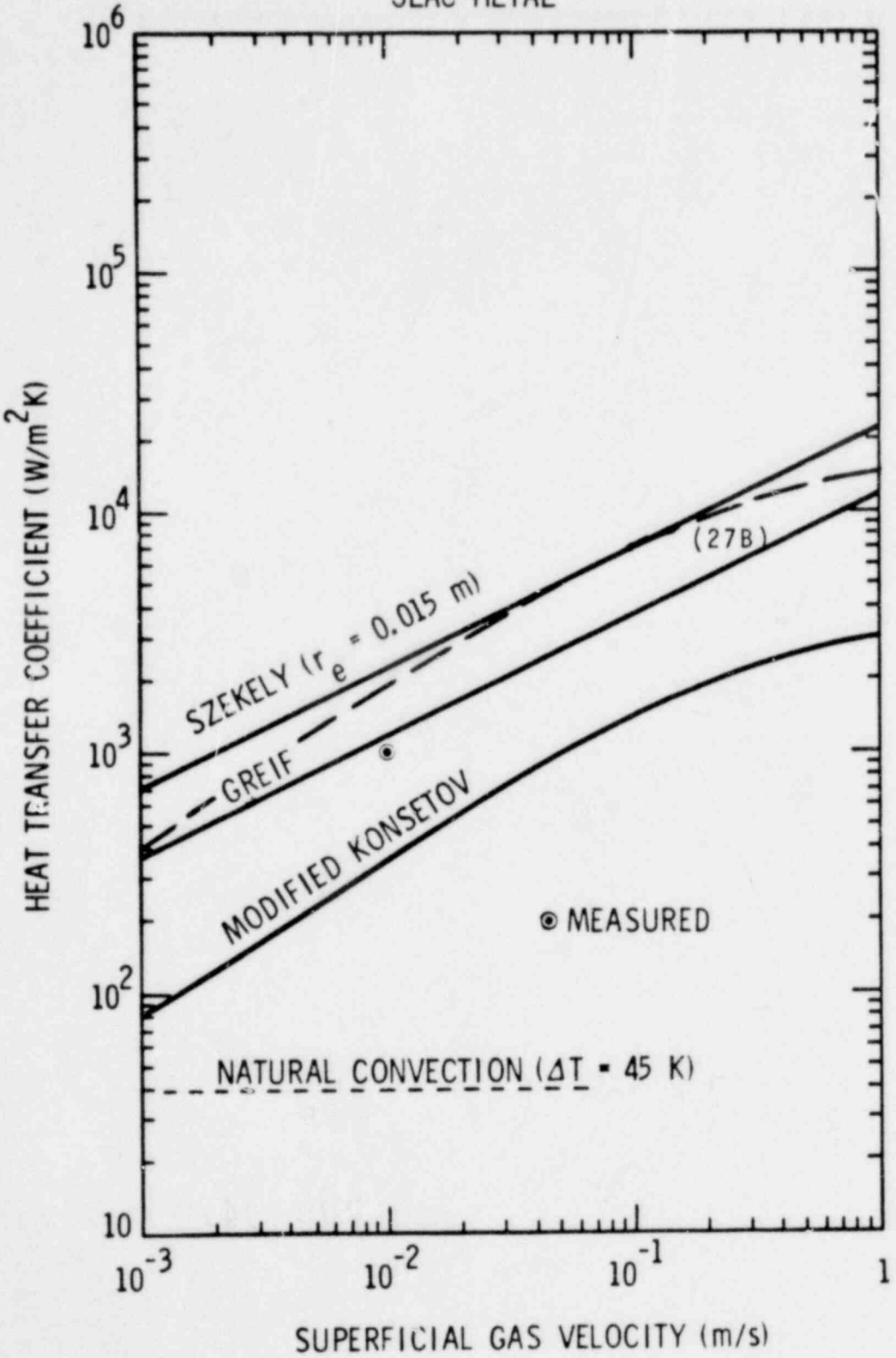

LIQUID/LIQUID INTERFACE

WITH BUBBLE AGITATION

OIL-WATER

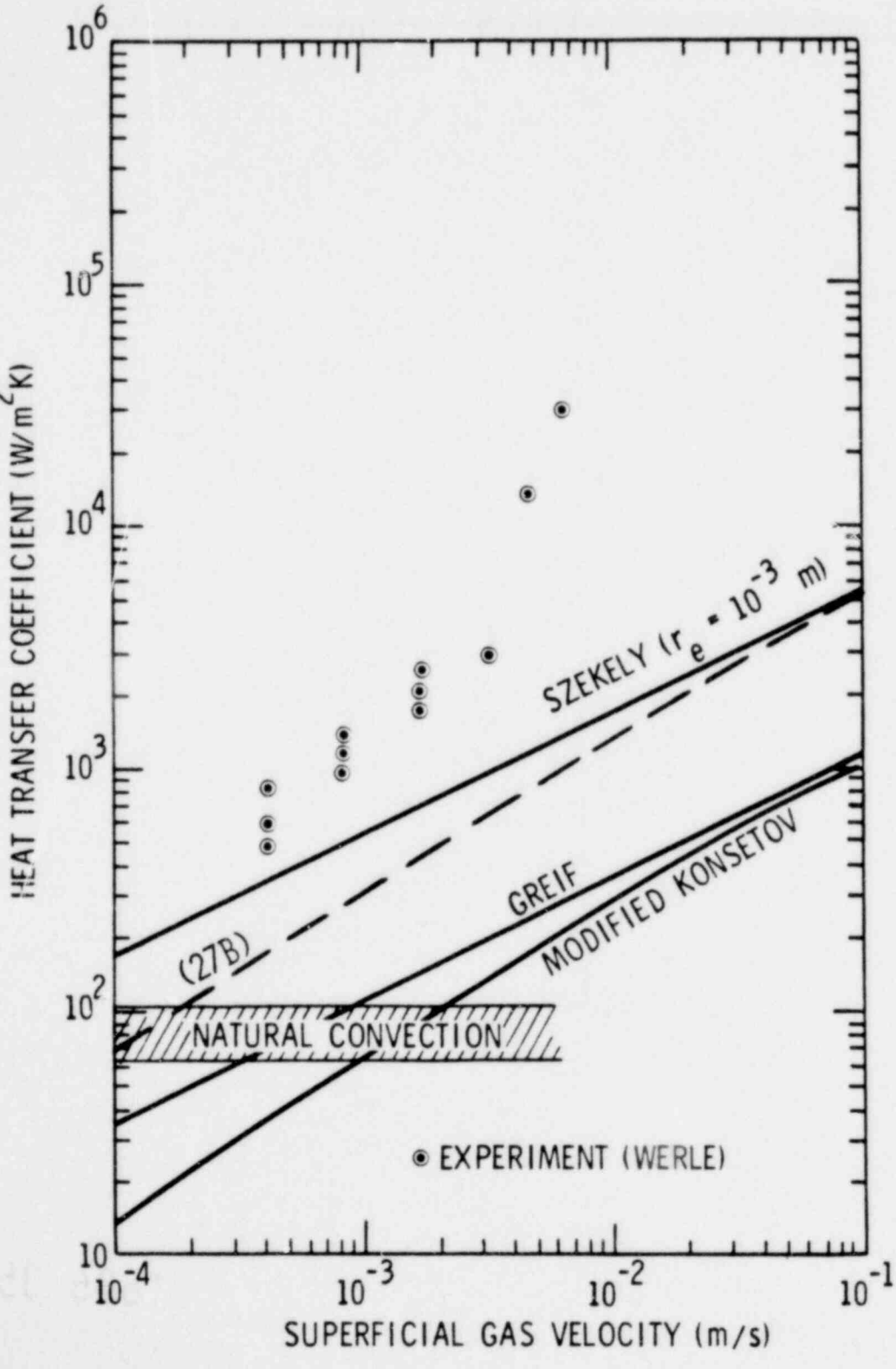

CONCRETE ABLATION

- STEADY-STATE, 1-D, MASS AND ENERGY BALANCES:

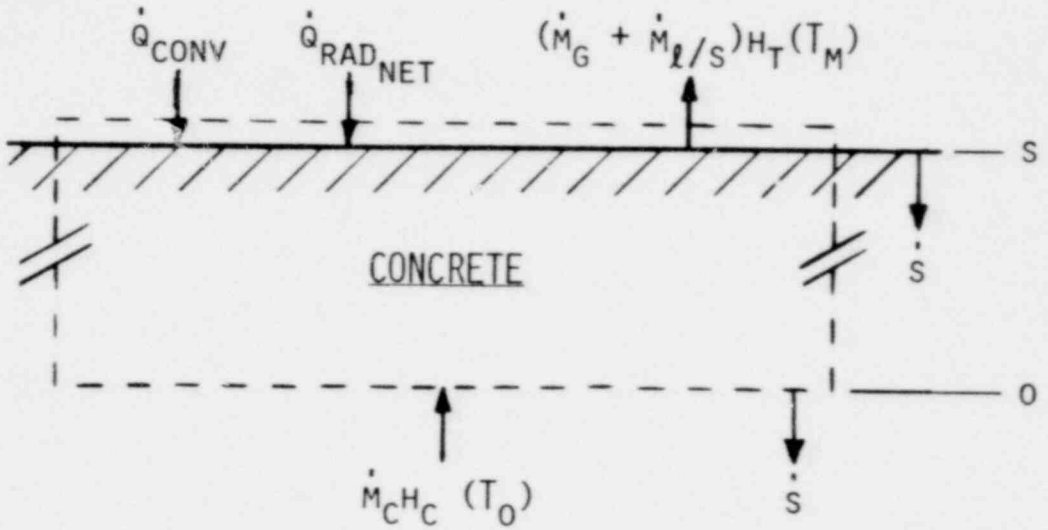

- MASS: $\dot{M}_G + \dot{M}_{\ell/S} = \dot{M}_C = \rho_C \dot{s}$

- ENERGY: $\dot{Q}_{CONV} + \dot{Q}_{RAD_{NET}} = \rho_C \dot{s}\left(H_T(T_M) - H_C(T_O)\right)$

CAVITY SHAPE CHANGE PROCEDURE

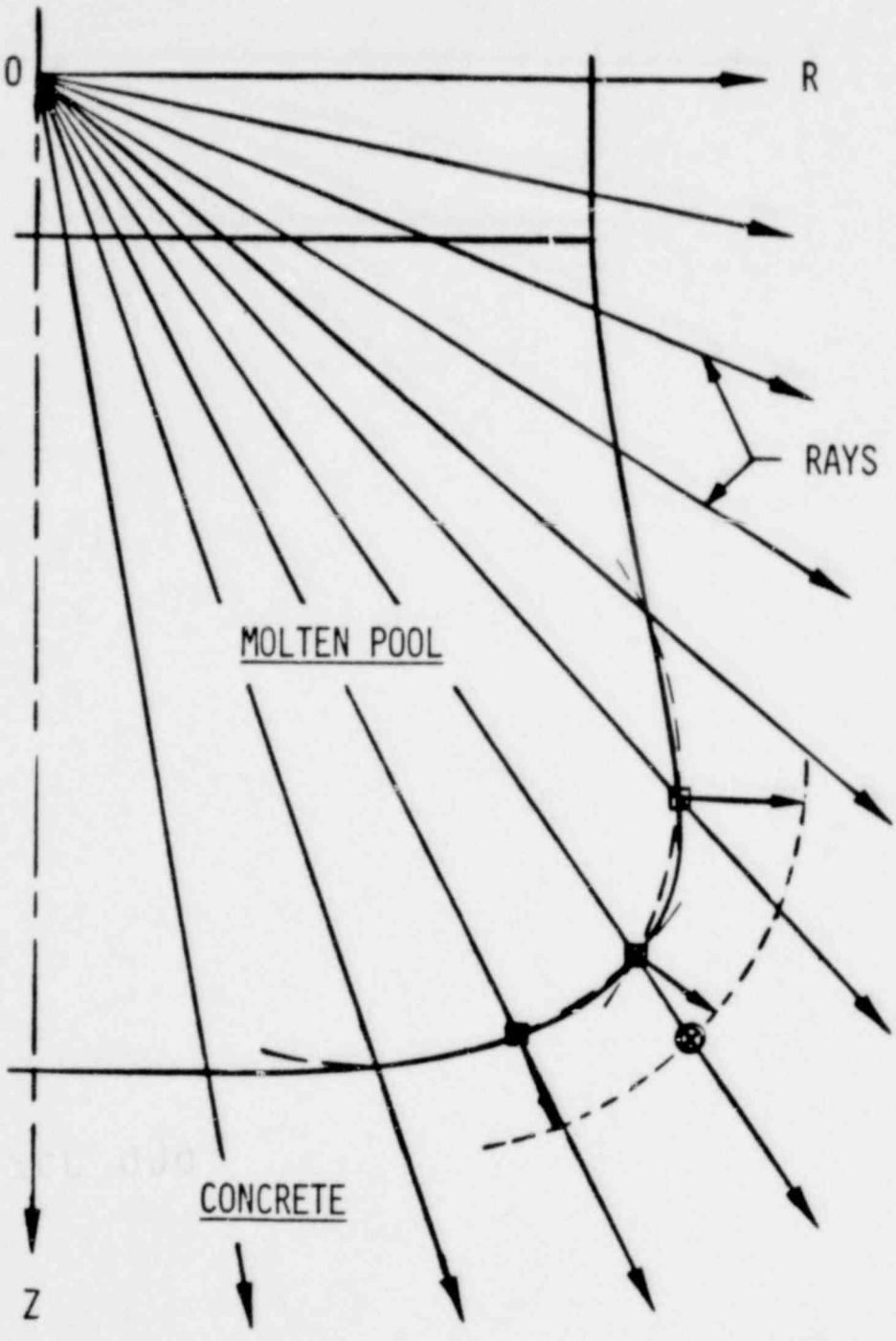

← OUTWARD NORMALS, ABLATION DEPTH

□ SURFACE POINTS AT TIME τ

● SURFACE POINT AT TIME $\tau + \Delta\tau$

EQUILIBRIUM SYSTEMS in CORCON

* GAS - METAL PHASES.

* GAS - OXIDE PHASES.

* GAS ABOVE MELT.

METHOD

FIRST-ORDER STEEPEST DESCENT

MINIMIZATION OF FREE-ENERGY.

SUBJECT TO:

* *STOICHIOMETRIC CONSTRAINTS*
* *NON-NEGATIVITY CONSTRAINTS*
* *CONSTANT TEMPERATURE*
* *CONSTANT PRESSURE*

CODE COMPARISON TEST ANALYSIS

- COIL TEST - INITIAL AND BOUNDARY CONDITIONS TO BE SUPPLIED TO CODE EVALUATORS DURING NOVEMBER:

  KFK - WECHSL
  SANDIA - CORCON
  KWU - KAVERN, BETZ
  UCLA - GROWS

- TEST PREDICTION/CODE COMPARISON CALCULATIONS -

  - EVALUATORS PROVIDED SAME AND SUFFICIENT INFORMATION ABOUT BOTH TESTS - COIL - SANDIA
    - SUPER-THERMITE - KFK

  - TEST RESULTS SUPPRESSED UNTIL PREDICTION COMPUTATIONS COMPLETED

- INTERACTION PARAMETERS PREDICTED TO INCLUDE:
  - CAVITY EROSION PROFILE
  - WEIGHT OF METALLIC PHASE
  - CONCRETE TEMPERATURE DISTRIBUTIONS
  - MELT PENETRATION VELOCITY
  - MELT SOLIDIFICATION TIME

- COMPUTATION RESULTS EXCHANGED WITH OTHER EVALUATORS

- ANALYSIS AND COMPARISON OF COMPUTED AND EXPERIMENTAL RESULTS

- DOCUMENTATION OF ANALYSIS RESULTS
  - DISTRIBUTION TO INTERESTED PARTIES